Journal of
Materials Chemistry C

Accepted Manuscript

This article can be cited before page numbers have been issued, to do this please use: Y. Lu, H. Yan, X. Meng, B. Li and S. Ge, *J. Mater. Chem. C*, 2017, DOI: 10.1039/C7TC03472E.

ROYAL SOCIETY OF CHEMISTRY

rsc.li/materials-c

View Article Online
DOI: 10.1039/C7TC03472E

Design, synthesis, photophysical properties and pH-sensing application of the pyrimidine-phthalimide derivatives

Han Yan, Xinlei Meng, Baoyan Li, Shusheng Ge, Yun Lu*

Department of Polymer Science and Engineering, State Key Laboratory of Coordination Chemistry, Collaborative Innovation Center of Chemistry for Life Sciences, Key Laboratory of High Performance Polymer Materials and Technology (Nanjing University), Ministry of Education, School of Chemistry and Chemical Engineering, Nanjing University, Nanjing 210093, P. R. China

*Author to whom correspondence should be addressed: Nanjing University, Nanjing 210023, China, E-mail: yunlu@nju.edu.cn

ABSTRACT

On the basis of molecular design about the donor-π-acceptor (D-π-A) pyrimidine-phthalimide derivatives, two new atypical AIE chromophores 2-(4,6-dimethylpyrimidin-2-yl)isoindoline-1,3-dione (**PB**) and 2-(4,6-bis(4-(dimethylamino)styryl)pyrimidin-2-yl)isoindoline-1,3-dione (**NPB**), were synthesized and characterized by using IR, ^{1}H NMR, ^{13}C NMR and HRMS. Both **PB** and **NPB** exhibited the obvious solid-state fluorescence emission due to their twisted geometries and positive solvatochromism due to their different molecular conformations in various solvents. Owing to the different push-pull electronic effects of substituents on the pyrimidine moiety, **PB** and **NPB**, acting as the D-π-A compounds, showed different HOMO-LUMO gaps and a variable red-shifted emission in their solid state, substantiating the possibility to tune effectively photophysical properties of these AIE chromophores by rational molecular design. In addition, **PB** and **NPB** could be easily and reversibly protonated at site of the nitrogen atoms, causing dramatic color changes. This phenomenon opened up the potential avenues of developing novel colorimetric pH sensors and logic gates for specific applications.

View Article Online
DOI: 10.1039/C7TC03472E

Introduction

The molecules with D-π-A structures, that is, connecting electron-donating (D) and electron-accepting (A) groups via a π-conjugated linker, have attracted increasing attention since they can serve as electroactive and photoactive materials in biochemical fluorescent technology,[1-4] efficient nonlinear optical (NLO),[5-7] electrogenerated chemiluminescence,[8-11] organic light-emitting diodes (OLEDs),[12-14] solar cells,[15-18] etc. Such functional molecular materials possess the intramolecular charge transfer (ICT) property, in which a number of functional donors (such as dimethylamino, diphenylamino, carbazoles, pyrroles, and dialkylamino) and acceptors (such as ketone, nitro, pyridine, and phthalimide) have been employed.[19]

Pyrimidine, as a heterocyclic molecule, has high electron affinity and good coplanarity, making it an appropriate building block in the construction of chromophores for optical sensors and pH-responsive materials.[20] The methyl groups located at positions 4- and 6- of the pyrimidine core have a well-known reactivity, and can easily undergo reaction with an aromatic aldehyde. Meanwhile, the amino group located at positions 2- can also be derivatized by many reactions, increasing not only the solubility of the molecule but also the extent of electron delocalization.

On the other hand, since aggregation-induced emission (AIE)[21,22] phenomenon was discovered, many organic molecules with AIE feature have been developed for the application of fluorescent sensors, cell imaging and organic light-emitting diodes.[23-28] In general, AIE-active molecules are characterized by the strongly twisted conformations, which enable them to emit more efficiently in the aggregated state by hindering intermolecular close stacking and intense π-π interaction.[29,30] Additionally, these molecules can also be explored further by the introduction of the appropriate functional units and used

View Article Online
DOI: 10.1039/C7TC03472E

as stimuli-responsive fluorescent solid-state probes for pH determination or solvent sensing.[31-34] Thus, AIE compounds have opened up a new path for the development of novel stimuli-responsive fluorescent materials. A series of molecules with AIE characteristics, such as 1-methyl-1,2,3,4,5-pentaphenylsilole (MPPS), tetraphenylethene (TPE), triphenylamine (TPA), etc. have been investigated in detail.[27,30] However, there are only limited reports on atypical AIE fluorescent materials because of the lack of clear guidelines on the structure-property relations of the molecules.[31-36]

In this work, we designed and synthesized two new atypical fluorescent molecules, 2-(4,6-dimethylpyrimidin-2-yl)isoindoline-1,3-dione (**PB**) and 2-(4,6-bis(4-(dimethylamino)styryl)pyrimidin-2-yl)isoindoline-1,3-dione (**NPB**), by attaching pyrimidine-based derivatives to the phthalimide moity. These two molecules have a similar framework of Y-shaped D-π-A chromophore structure, in which the *N*,*N*-dimethylaniline units acted as donors and the pyrimidin derivative moiety as an acceptor. The effect of difference in electropositivity for two groups (methyl and *N*,*N*-dimethylaniline) in **PB** and **NPB** respectively on the AIE activity was investigated, and for these as-prepared new functional molecules, their solvatochromic properties, nanoaggregates, the response to pH and the potential application in logic gates, as well as the theoretical calculation about structures were studied as well.

Results and discussion

Synthesis

In this work, two new chromophores, **PB** and **NPB**, consisting of the phthalimide and pyrimidine-based derivatives were synthesized (Scheme 1). The reaction was carried out under refluxing conditions in toluene, and products were readily obtained by recrystallization in good yield. Also, the procedure is simple and convenient. All the intermediates and final

View Article Online
DOI: 10.1039/C7TC03472E

products were carefully purified and fully characterized by IR, ^{1}H NMR, ^{13}C NMR and HRMS, which confirmed their expected molecular structures. These compounds were found to be soluble in common organic solvents such as CH_2Cl_2, $CHCl_3$, toluene, DMF, but insoluble in methanol and water.

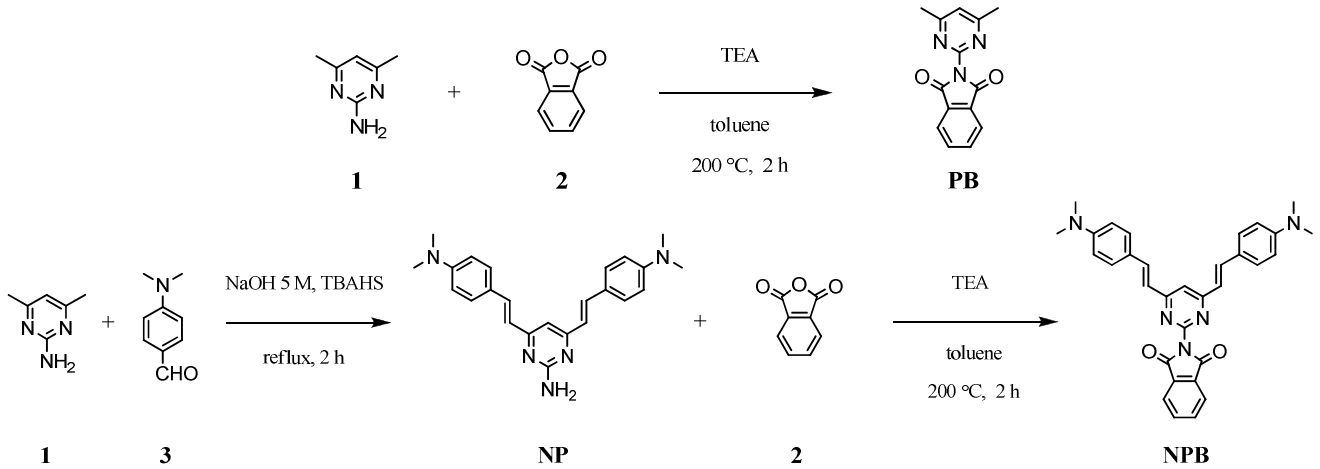

Scheme 1 Synthetic routes to **PB** and **NPB**.

Thermal stability

Thermal stability is one of the key requirements for practical applications of organic fluorophores. It can be seen that, from the thermogravimetric analysis (TGA) curves (Fig. S1, see Supporting Information), the degradation temperatures (T_d) of 5% weight loss of the **PB** and **NPB** were 210 and 345 °C respectively. There was a total loss of about 40% for **NPB** when being heated to close to 400 °C. **NPB** exhibited a higher stability due to its more planar molecular configuration, which led to a longer conjugation length and stronger intermolecular interactions. The results indicated that such pyrimidine-phthalimide derivatives can provide desirable thermal properties through rational molecular structure design.

AIE properties

View Article Online
DOI: 10.1039/C7TC03472E

Both **PB** and **NPB** showed the solid-state emission maxima under UV light of 365 nm and the fluorescence emission peaks for their respective crystals and powders were located at 512 and 621 nm, respectively (Fig. 1a). Their solid-state fluorescence observed could be ascribed mainly to contribution of the whole twisted molecular structure. Compared to **PB**, **NPB** showed a red-shifted emission peak due to the replacement of the strong electron-donating groups *N*,*N*-dimethylaniline units on the 4- and 6- position of the pyrimidine core and the enlarged conjugation segment by C=C bond linked with the *N*,*N*-dimethylaniline units and pyrimidine core. Different samples gave varied fluorescence quantum yields (Φ) such as 0.35 for **PB** crystal, 0.31 for **PB** powder, 0.44 for **NPB** crystal and 0.43 for **NPB** powder. The CIE chromaticity coordinates of **PB** and **NPB** were depicted in Fig. 1b, and their values were calculated to be (0.1662, 0.6322) and (0.5988, 0.3237) respectively, which were consistent with the colors displayed by these two chromophores.

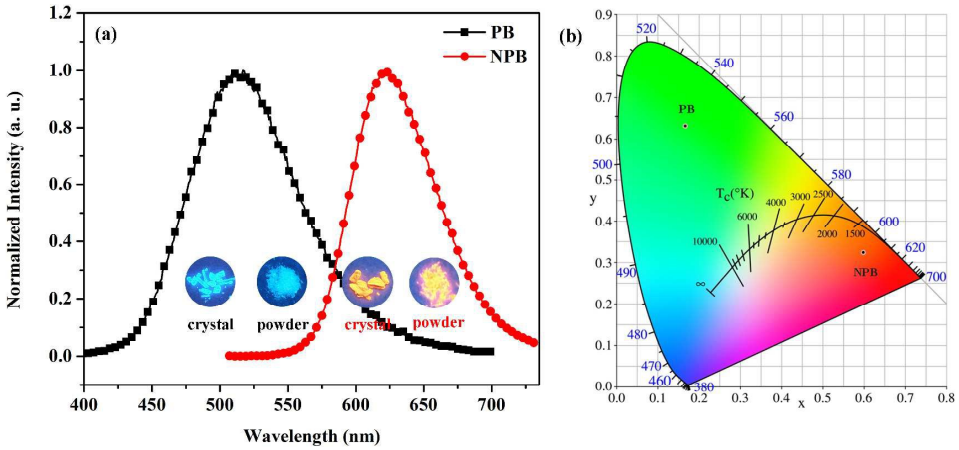

Fig. 1 (a) Solid-state photoluminescence (PL) spectra (λ_{ex} = 365 nm), inset: photo images of the powder solids and crystals for **PB** and **NPB** respectively (λ_{ex} = 365 nm). (b) Commission Internationale de l'Eclairage (CIE) chromaticity coordinates of **PB** and **NPB**.

We used THF and water respectively as good and poor solvent for further investigating

View Article Online
DOI: 10.1039/C7TC03472E

the aggregation-induced emission of **PB** and **NPB**. Fig. 2 showed the PL spectra and the change in fluorescence intensity of **PB** and **NPB** in various water-THF mixtures. In the case of **PB**, its pure THF solution emitted weak blue light, which was ascribed to the free rotation of pyrimidine ring and phthalimide ring around the C-C bond facilitating a non-radiative relaxation process. As water was gradually added to the THF solution, the PL intensity of **PB** molecules displayed first the drop, then the rise, and then again the fall (Fig. 2a and 2b). The enhanced PL intensity with increasing water fraction (f_w) to 50% indicated that the dissolved molecules began to aggregate with a restriction of intramolecular motion (RIM) process resulting in obvious aggregation-induced emission. The luminescence behavior of **PB** molecules that showing a decrease rather than increase in intensity at $f_w < 10\%$ is hard to explained and the cause was unclear. For the phenomenon of lowering again the PL intensity at $f_w > 50\%$, a possible reason was that at higher water content, molecules come out from the solvent and tend to aggregate, which in turn creates a nonpolar microenvironment around the molecules thus decresing the fluorescence.[37-39] In the case of **NPB**, its AIE-behavior was found to be different to that of **PB** (Fig. 2c and 2d). The PL intensity remained unchanged below the f_w values of 30%. Due to the introduction of the polar groups *N*,*N*-dimethylaniline units, **NPB** exhibited a relative higher solubility in the solvents with low water fraction than **PB**, that could be why the emission spectra of **NPB** were not affected dramatically by solvent effect with the increase of water fraction. Then the PL intensity continues to increase suddenly until the f_w of 50%, and after that the rate of increase slowed down. Obviously, the pronounced fluorescence enhancement phenomenon could be interpreted as the aggregation of **NPB** at higher f_w values. According to the RIM mechanism, when **NPB** was dissolved in THF or THF/water mixtures with a relative high ratio, the active intramolecular rotations of dimethylamino groups and phthalimide ring exhausted the energy of the molecules under

View Article Online
DOI: 10.1039/C7TC03472E

excited state and resulted in fluorescence quenching. When more water was added into the solution, **NPB** tended to form aggregates, in which the intramolecular rotations were restricted and the excited states were decayed to the corresponding ground states through irradiative channels.[40] In such case, relative to **PB**, the enlarged molecular structure and twisted conformation of **NPB** molecules increased steric hindrance and reduced intermolecular contact, thus prevented redundant π-π stacking and presented the AIE behavior.

Except for the short wavelength (SW) peaks ranging from 400 to 470 nm, it is also noticed that long wavelength (LW) peaks at 619 nm appeared in the PL spectra of **NPB** in the aqueous mixtures (Fig. 2c). According to the reported literature,[41] the phthalimide moiety and the pyrimidine derivative groups may affect respectively the SW and the LW excited-state energy levels. Thus it is believed that the LW peak was probably associated with the TICT emission of the enlarged conjugation pyrimidine unit, and/or the equilibrium between the AIE and the TICT in the excited state of **NPB** molecules.

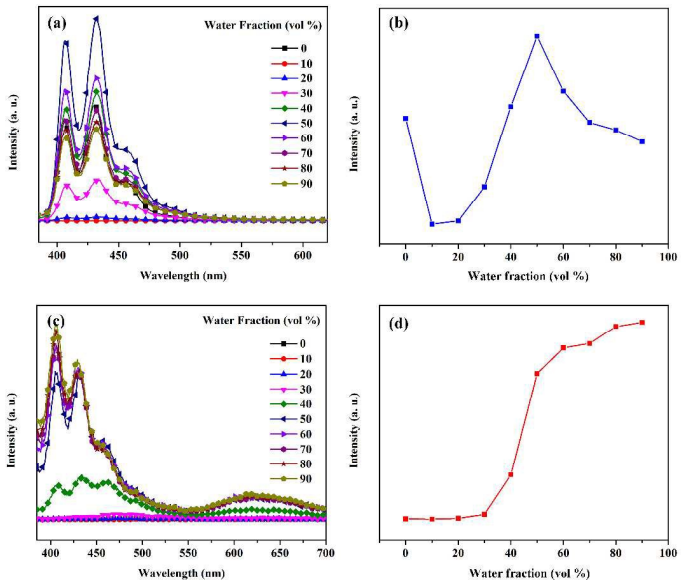

Fig. 2 PL spectra of (a) **PB** and (c) **NPB** in water-THF mixtures with different ratios, and the

View Article Online
DOI: 10.1039/C7TC03472E

corresponding plot of fluorescent intensity against f_w of (b) **PB** and (d) **NPB**. (λ_{ex} = 365 nm).

In addition, the SEM images showed that below f_w = 10% (**PB**, Fig. 3a) and 0% (**NPB**, Fig. 3c), regular large quadrate and block-plate like nanoparticles formed, meaning that **PB** and **NPB** had sufficient solubility in THF / THF with low water fraction. Attributing to the slow process of molecular aggregation, ordered assemblies based on the π-π interactions between molecules could be generated, as a result, the detrimental species of excimers formed and led to the fluorescence weakening.[42] And at f_w = 90%, few ordered microstructures were observed for both **PB** (Fig. 3b) and **NPB** (Fig. 3d). At this point, the molecules became insoluble and aggregated quickly so that no time to arrange in a regular π-π packing mode. In such case, the resulted restriction of intramolecular rotation effect was most responsible for the AIE behavior and the enhenced fluorescence emission.

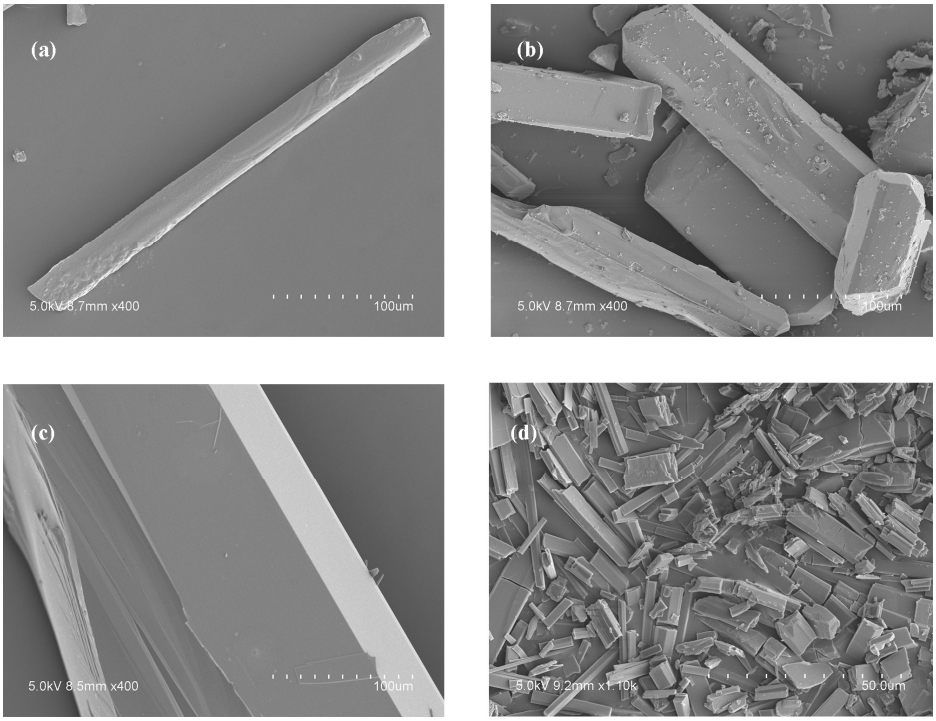

Fig. 3 SEM images for the solids formed by **PB** and **NPB** in THF/water mixtures with different f_w. (a) **PB**, f_w = 0%; (b) **PB**, f_w = 90%, (c) **NPB**, f_w = 0%, and (d) **NPB**, f_w = 90%.

View Article Online
DOI: 10.1039/C7TC03472E

Crystalline Characteristic

Determination of X-ray single-crystal structures is the most effective and powerful tool for acquiring the ground-state molecular structures and revealing the AIE mechanism. As shown in Fig. 4a, the X-ray crystal structure of **PB** was found to be triclinic with space group as $\bar{P}1$. The dihedral angle angle between the adjacent rings A and B was 69.96°. Upon aggregating, these intramolecular rotations were highly restricted, thus enhancing the observed fluorescence emission. The stacking structures of **PB** in the crystals were shown in Fig. 4a, except partial antiparallel π···π stacking interaction between pyrimidine rings separated at a distance of 4.03 Å, few intermolecular π-π stacking was observed due to the twisted arrangement.[43] Such aggregation mode could be classified as J-aggregate. Therefore, the twisted geometry had important influence on the AIE property, in which the J-aggregate formation probably caused the further increase of the emission intensity.[44]

A similar type of randomness was absent in **NPB** also mainly due to its twisted structure. The dihedral angle angle between the adjacent rings C and D was 75.88° (Fig. 4b). **NPB** molecules aligned themselves in antiparallel geometry in adjacent layers with a small partial π-overlap between the aromatic units due to the J-aggregate packing (Fig. 5b). The layers were separated by a distance of 3.98 Å. Herein, the AIE of **PB** and **NPB** can be attributed to their twisted conformations, which were conducive to prevent the formation of excimers or exciplexes and boost the emission of samples in the aggregate state.

View Article Online
DOI: 10.1039/C7TC03472E

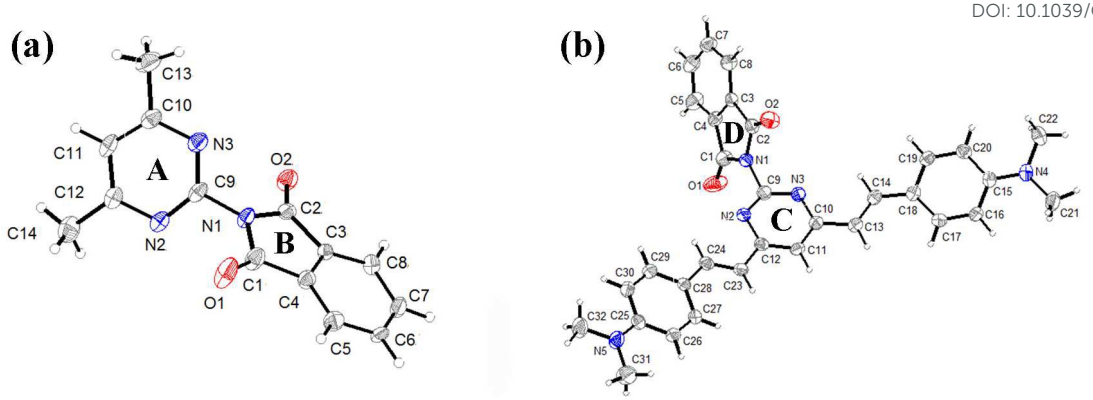

Fig. 4 Molecular structure (ORTEP diagram) of (a) **PB** and (b) **NPB**.

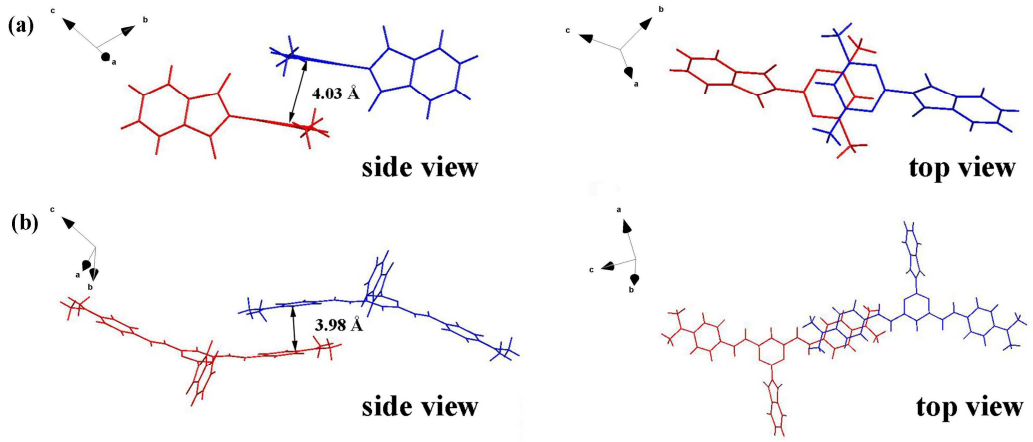

Fig. 5 Packing structure of (a) **PB** and (b) **NPB** single crystal.

Solvent induced emission changes

The donor-acceptor property of **PB** and **NPB** in various solvents was exhibited in their characteristic dual-band absorption spectra where the high energy band was attributed to the π→π* transition and the low energy band ascribed to intramolecular charge transfer transition. Compared to **PB**, the absorption of **NPB** ranging from 271 to 403 nm indicated that the proposed D-π-A compound **NPB** is able to absorb over an extended absorption range, leading to excellent light-harvesting. Moreover, absorption spectra of **PB** and **NPB** were not dramatically solvent-dependent, implying that the effect of solvent polarity was negligible for the molecules in the ground state.

View Article Online
DOI: 10.1039/C7TC03472E

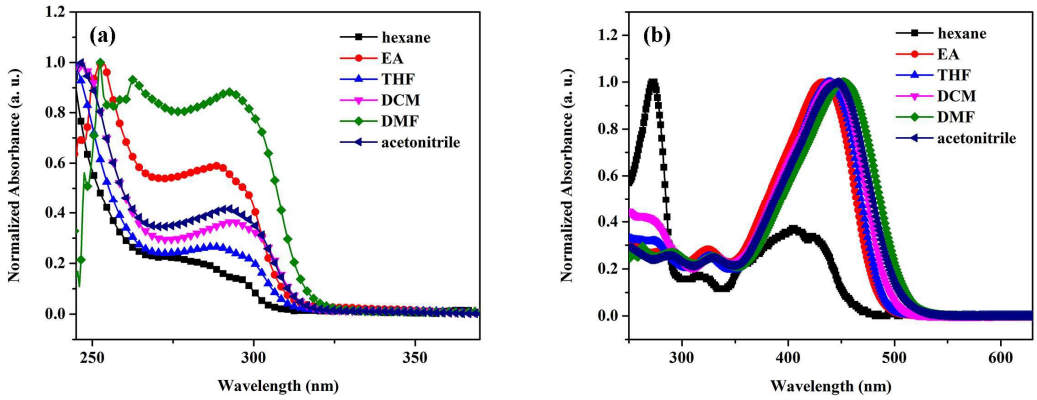

Fig. 6 UV-vis absorption spectra of (a) **PB** and (b) **NPB** in various solvents.

The emission behaviors of **PB** and **NPB** in solvents with different polarities were checked as shown in Fig. 7. In non-polar hexane, **PB** showed an emission with a peak at 402 nm and two vibronic couplings at 387 and 428 nm, which indicated three close-lying excited vibration states with small energy gap. With the increasing the solvent polarity, red-shifted emissions with varying degrees were observed in mid-polar solvents (EA, THF and DCM) and polar solvents (DMF and acetonitrile), suggesting the presence of positive solvatochromism (Fig. 7a). In addition, a single fluorescence emission peak in EA and DCM as well as a dual peak in THF, DMF and acetonitrile with different red shift were observed. Among the dual peak, the one at shorter wavelength (400 ~ 420 nm) could be assigned to the contribution of the locally excited (LE) state, while the one at longer wavelength (435 ~ 474 nm) could be ascribed to that of twisted intermolecular charge transfer (TICT) state.[45] The variation of the PL spectra for **PB** with the change of solvent polarity probably related to the potential energy surfaces of the molecule in diverse settings (Fig. 8). As a D-π-A system, **PB** is in the LE state with the lowest energy in nonpolar solvents, and its emission came mainly from the LE state. With the increase in polarity of the solvent, the TICT state with higher energy is stabilized by solvation of the polar solvents, making the energy level of two states

View Article Online
DOI: 10.1039/C7TC03472E

closer to each other. The red shift of emission peak in the PL spectra in solvents with medium polarity such as THF and DCM just reflected the presence of TICT state. Especially, in the high polar solvents such as DMF and acetonitrile, the level of TICT state became even lower than that of the LE state and thus the emission was mainly from the TICT state.[46] At this point, due to the intramolecular rotation caused by dipolar solute-solvent interactions, the energy level of **PB** completed its transformation from the LE to the TICT state after the total charge separation between the donor and acceptor units was completed. The resulting twisted conformation was stabilized by surrounding polar solvents, leading to the narrowed band gap and consequently large red-shifts of 130 nm in the PL spectra.[47] Compared with **PB**, the PL spectra of **NPB** exhibited a larger red-shift in their maxima with increasing solvent polarity (Fig. 7b). This indicated that due to introduction of the *N*,*N*-dimethylaniline groups acted as a strong donor, the stronger push-pull effect made molecular dipole moment in the excited state much larger than that in the ground state.

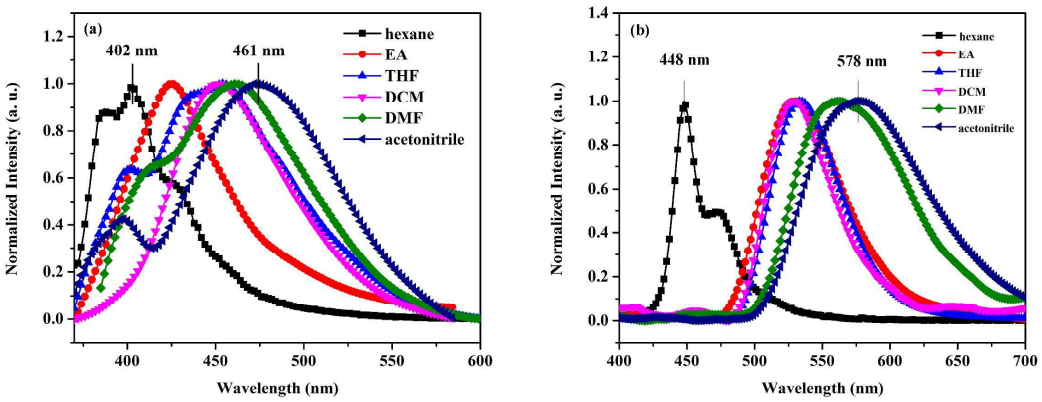

Fig. 7 Normalized PL spectra of (a) **PB** and (b) **NPB** in various solvents (5×10^{-5} M). λ_{ex} = 365 nm.

View Article Online
DOI: 10.1039/C7TC03472E

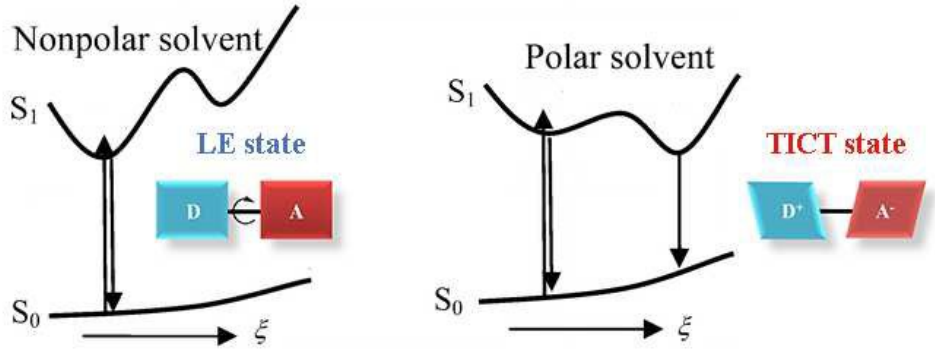

Fig. 8 Schematic of the potential energy surfaces describing the LE→TICT reaction.

In order to further reveal the polarity effect on the molecular excited state relaxation and the fluorescence property, **NPB** was chose to measure its PL spectra in the mixed solvents due to its larger positive solvatochromism effect relative to **PB**. As shown in Fig. 9, with titrating EA into dilute hexane solution of **NPB** (~10^{-5} M), the two peaks (448, 476 nm) decreased gradually, and at the same time the peak at 454 nm with a relative lower intensity emerged and also red-shifted as the ratio of EA to hexane increased. This fact indicated that, for **NPB**, its emission band position is very sensitive to the solvent polarity (just with a little amount of polar solvent) due to the ICT character of the excited state.

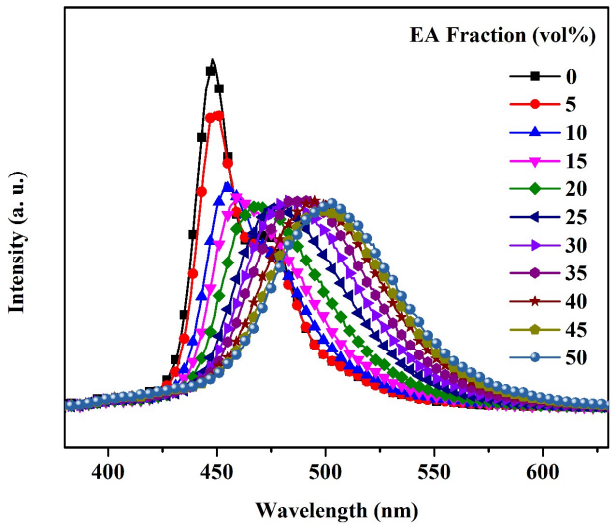

Fig. 9 PL spectra of **NPB** in mixed solvents mixing hexane (5×10^{-5} M) with EA. $\lambda_{ex} = 365$ nm.

View Article Online
DOI: 10.1039/C7TC03472E

Further, the photophysical data of **PB** and **NPB** in different solvents were summarized in Table 1. The results showed that **PB** possessed the highest quantum yield of 14% in DCM and the lowest one of 0.5% in hexane. The results may be relative to the equilibrium between the LE and the TICT state in the excited state.[48] When in nonpolar or midpolar solvents (hexane, EA, THF and DCM), **PB** is mainly LE state which has a fast radiative rate constant causing the high quantum yields. As the solvent polarity increased, the equilibrium shifted to the TICT state, emission intensity was normally weakened because of the susceptibility of the TICT state to various nonradiative quenching processes,[49] which explained the low quantum yield of **PB** in DMF and acetonitrile. Similar quantum yield change was observed for **NPB**, here we just discussed the photophysical data of **PB** as an example.

Table 1. Photophysical data of **PB** and **NPB** in various solvents.

solvent	**PB**				**NPB**			
	λ_{ab} (nm)	λ_{em} (nm)	Stoke's shift (cm^{-1})	Φ*	λ_{ab} (nm)	λ_{em} (nm)	Stoke's shift (cm^{-1})	Φ*
hexane	286	402	10089	0.005	398	448	2805	0.005
EA	289	425	11072	0.065	399	532	6266	0.072
THF	291	450	12142	0.071	399	533	6301	0.085
DCM	293	453	12130	0.142	399	533	6301	0.200
DMF	293	462	12485	0.032	400	563	7238	0.042
acetonitrile	293	474	13033	0.024	400	578	7699	0.035

* The quantum yield (Φ) was measured by using the quinine sulfate solution (in 0.1 M

View Article Online
DOI: 10.1039/C7TC03472E

H_2SO_4, literature quantum yield 54% at 360 nm) as the standard and calculated with the equation of $\Phi = \Phi_R (I/I_R)(A_R/A)(n^2/n_R^2)$. Where, Φ_R is the quantum yield, I is the measured integrated emission intensity, n is the refractive index, A is the optical density and the subscript R refers to the quinine sulfate.

The effects of solvents on the emission features could be further evaluated by the direct correlations between the solvent polarity parameter (Δf) and Stokes shift of the absorption and also emission maxima via Lippert-Mataga equations of $\Delta\upsilon = \Delta\upsilon_{abs} - \Delta\upsilon_{em} = \frac{2\Delta f}{hca^3}(\mu_e - \mu_g)^2 + \text{constant}$ (1) and $\Delta f = f(\varepsilon) - f(n^2) \approx \frac{\varepsilon - 1}{2\varepsilon + 1} - \frac{n^2 - 1}{2n^2 + 1}$ (2),[50] where $\Delta\upsilon$ was the Stokes shift; $\Delta\upsilon_{abs}$ and $\Delta\upsilon_{em}$ were wavenumbers of the absorption and fluorescence peaks; h was Planck's constant; c was the velocity of light; a was Onsager cavity radius; μ_e and μ_g were the excited and ground state dipole moments; Δf was the orientational polarizability of solvent which could be calculated using the dielectric constant e and refractive indices n of the solvent. The plot ($\Delta\upsilon$-Δf) for both **PB** and **NPB** exhibited a linear relationship (Fig. 10), suggesting that the dipole-dipole interaction between the solute and solvent were mainly responsible for the solvent-dependent fluorescence shift. In addition, the slopes of the fitting line for **PB** and **NPB** were as high as 4389 and 9300, respectively. **NPB** exhibited much larger slope than **PB**, suggesting its larger dipole moment changes between the ground and excited states (μ_e-μ_g) under photoexcitation. The result revealed that **NPB** had an extremely polar structure in the excited state and stronger TICT effect, which were beneficial to nonlinear optical properties.[51]

View Article Online
DOI: 10.1039/C7TC03472E

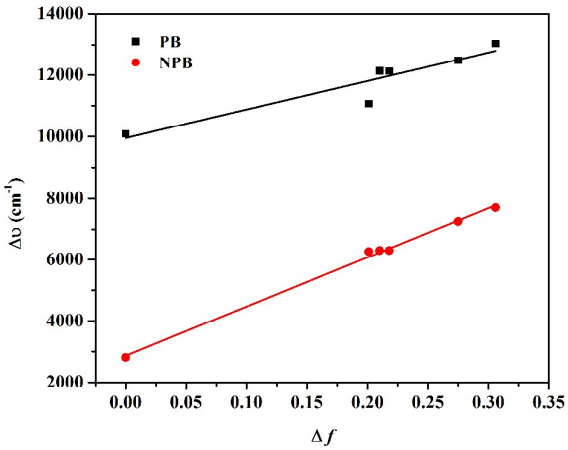

Fig. 10 Lippert-Mataga solvent polarity graphs for **PB** and **NPB**.

Electronic Structure.

The density functional theory (DFT) computation technique[52] has been used to optimize the geometries of **PB** and **NPB**, and the highest occupied molecular orbital (HOMO) and lowest unoccupied molecular orbital (LUMO) were shown in Fig. 11. The HOMO for PB was distributed on the 4,6-dimethylpyrimidine unit and parts of the phthalimide moiety, whereas the HOMO for **NPB** was distributed on the *N*,*N*-dimethylaniline units and C=C bond. In view of the fact that the LUMO, for both **PB** and **NPB**, was mainly distributed over the phthalimide moiety, the HOMO and LUMO energy levels were well separated which was in favor of a facile charge migration.[53] In addition, the theoretical HOMO-LUMO gap for **PB** and **NPB** were 3.394 eV and 1.897 eV respectively, verifying the status for both **PB** and **NPB** as D-π-A compounds. Besides, the bandgap value of **NPB** was a lower comparing with that of **PB**, indicating its larger delocalization and push-pull effect.

View Article Online
DOI: 10.1039/C7TC03472E

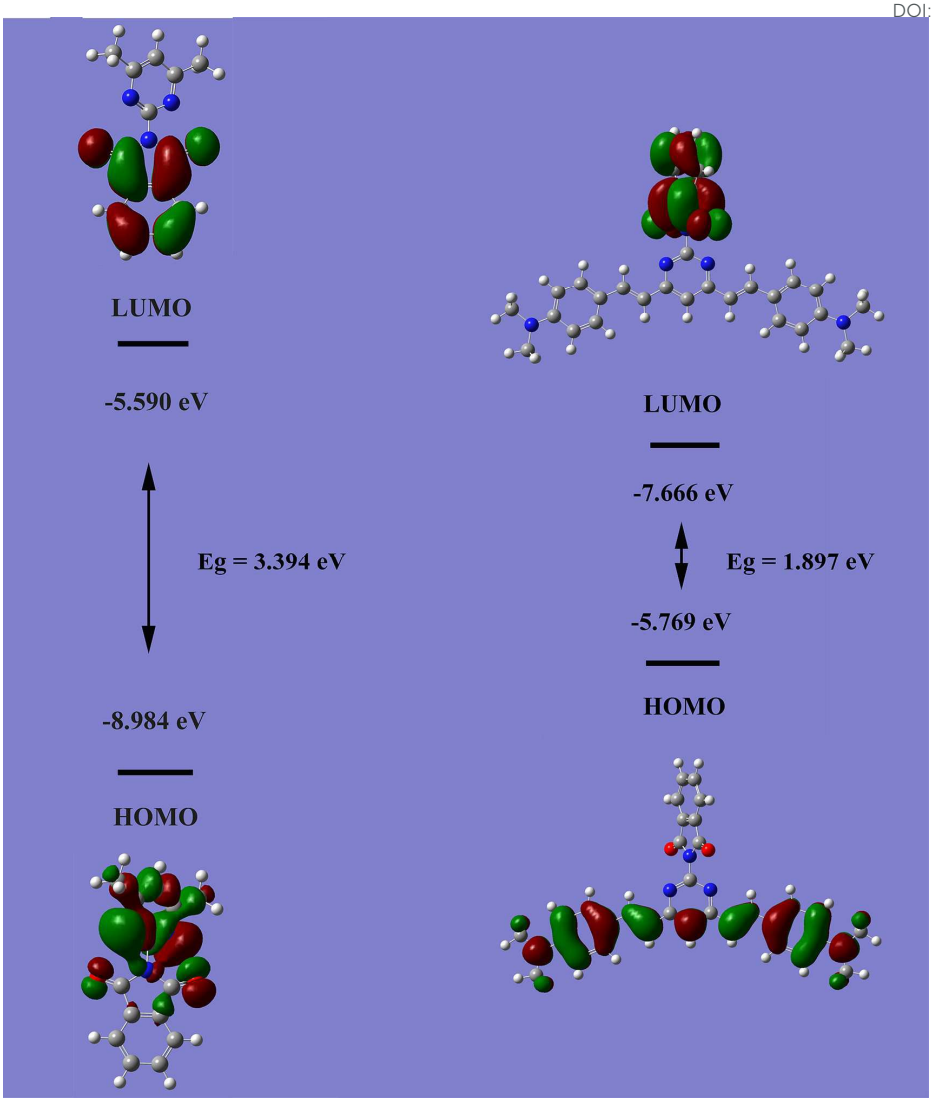

Fig. 11 B3LYP/6-31G(d) calculated molecular orbital amplitude plots and energy levels of the HOMOs and LUMOs of **PB** and **NPB**.

pH sensing

The nitrogen atoms of the as-prepared pyrimidine units are alkaline centers that can be protonated. Thus, the effect of protonation on the optical properties of **PB** and **NPB** with pyrimidine structure was also studied. As **PB** and **NPB** solutions in DCM experienced a acidification by the addition of TFA (Fig. 12), a fully reversible change can be observed after a subsequent neutralization with base (Et_3N), and the cycle depicted can be repeated at least 10 times without loss of sensitivity to pH change.

View Article Online
DOI: 10.1039/C7TC03472E

Instrestingly, the absorbance change of **PB** induced by TFA was much smaller than that of **NPB** and only the **NPB** solution turned its colors from yellow to dark brown then to blue with increasing concentration of TFA, indicating that **NPB** was quite a sensitive probe for acid detection in naked-eye observation. The changes observed in the PL spectra of **PB** upon addition of acid are illustrated in Fig. 12a. The increase in the concentration of TFA led to the appearance of a new, about 10 nm red-shifted band corresponding to the protonated species, undergoing a slight color change. This bathochromic shift can be explained by an increased charge transfer from the new D-π-A system in which dimethyl groups acted as weak donor and remanent protontated moity acted as accepter (Fig. 14a). In the case of **NPB**, the emission (Fig. 13) is a consequence of radiative deactivation from both excited TICT and LE state at this particular concentration.[54] On addition of TFA, the nitrogen atoms at position 1- and 3- of the pyrimidine unit and phthalimide moiety were first protonated (Fig. 14b), thus the effect of acceptor part increased, the push-pull effect got stronger and TICT became more prominent, consequently, the fluorescence color of the solution changed from yellow to orange. Compared to **PB**, not only the nitrogen atoms at position 1- and 3- of the pyrimidine ring and phthalimide moiety but also the two dimethyl amino groups can be protonated, as a result, the push-pull effect was destroyed because the further protonated **NPB** was no longer a D-π-A molecule, the emission came mainly from the LE state and the fluorescence color of the solution changed in turn to dark blue. In this case, upon further addition of TFA, a new, more intense blue-shifted band emerged at 457 nm corresponding to the protonated species.

View Article Online
DOI: 10.1039/C7TC03472E

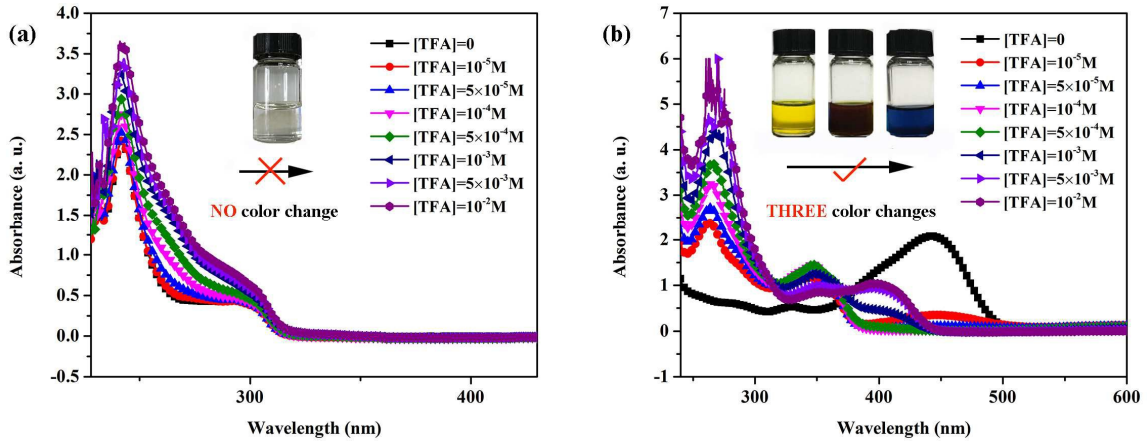

Fig. 12 Changes in the absorbance of (a) **PB** and (b) **NPB** (5×10^{-5} M in DCM) with increasing concentration of TFA.

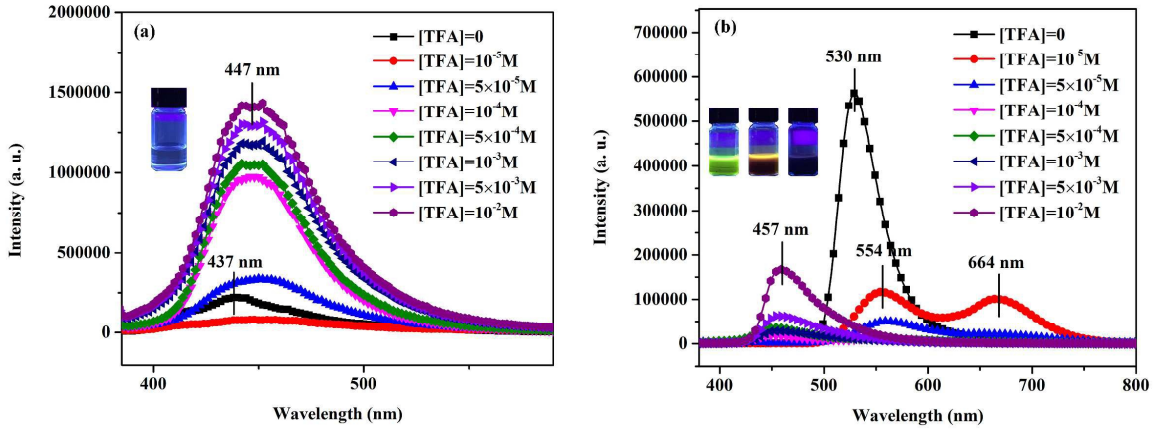

Fig. 13 Changes in the PL intensity of (a) **PB** and (b) **NPB** (5×10^{-5} M in DCM) with increasing concentration of TFA. $\lambda_{ex} = 365$ nm.

View Article Online
DOI: 10.1039/C7TC03472E

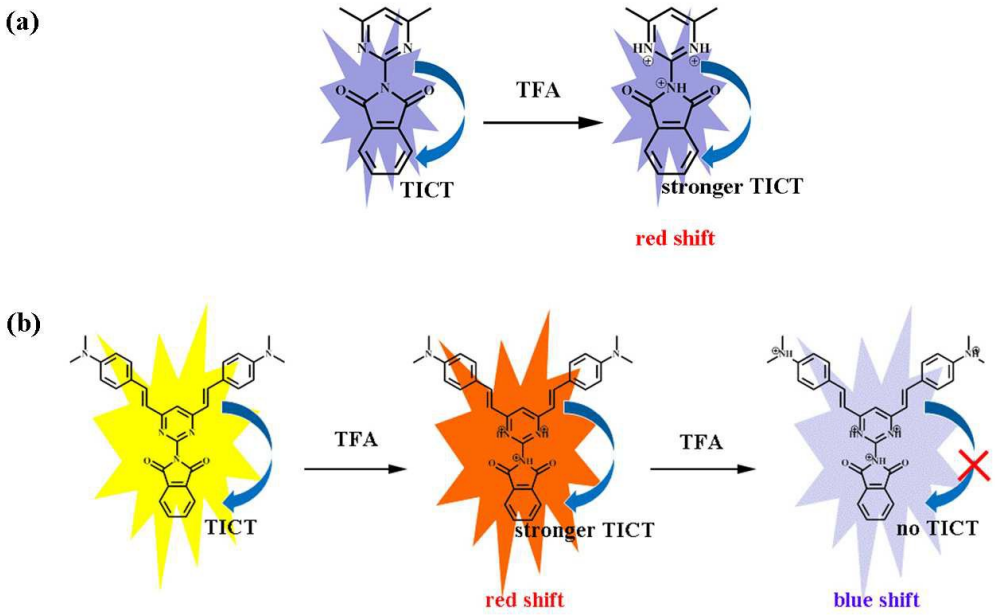

Fig. 14 The pH-sensing mechanism of (a) **PB** and (b) **NPB** (5×10^{-5} M in DCM) with increasing concentration of TFA.

The optical performance of **PB** and **NPB** in the solid state is also sensitive to change in surrounding TFA vapor. **PB** and **NPB** were wrote onto a non-emissive filter paper when exposed to TFA vapor for 30 min and 5s, respectively (Fig. 15). Consequently, the track with blue-green fluorescence for **PB** was almost unchanged while the track with orange fluorescence for **NPB** was changed to green under day light and quenched under 365 nm ultraviolet. The result indicated that the solid state of **NPB** was quick responsive to TFA atmosphere.

To understand the fluorochromic mechanism for **PB** and **NPB** in the presence of pH stimuli, PXRD measurements were carried out (Fig. 16). When **PB** and **NPB** were exposed to TFA vapor, only the liquid film for **NPB** was rapidly formed because the protonated **NPB** was hard to be solidified just as many quaternary ammonium ionic liquids, which may be resulted from the collapse of crystalline lattices induced by the protonation. The fluorescence emission of **NPB** was switched off under acid stimuli, also due to the deaggregation of AIE

View Article Online
DOI: 10.1039/C7TC03472E

gens or destruction of the ICT process. Furthermore, it was found that the color of **PB** neither under day light nor 365 nm ultraviolet showed any change in presence of TFA vapor, implying that the quenched fluorescence in the solid state should be ascribed to protonation of dimethylamino rather than the pyrimidin unit. Indeed, the protonated dimethylamino loses its ability to construct a D-π-A system and turns **NPB** to a non-emissive phase. Within this context, the **NPB** could recognize TFA vapor with a detection limit of 20 ppm, exhibiting a clear colorimetric response to an acid environment–both in solution and in the gas phase. Such excellent pH-sensing property made **NPB** promising for developing some smart materials in the further.

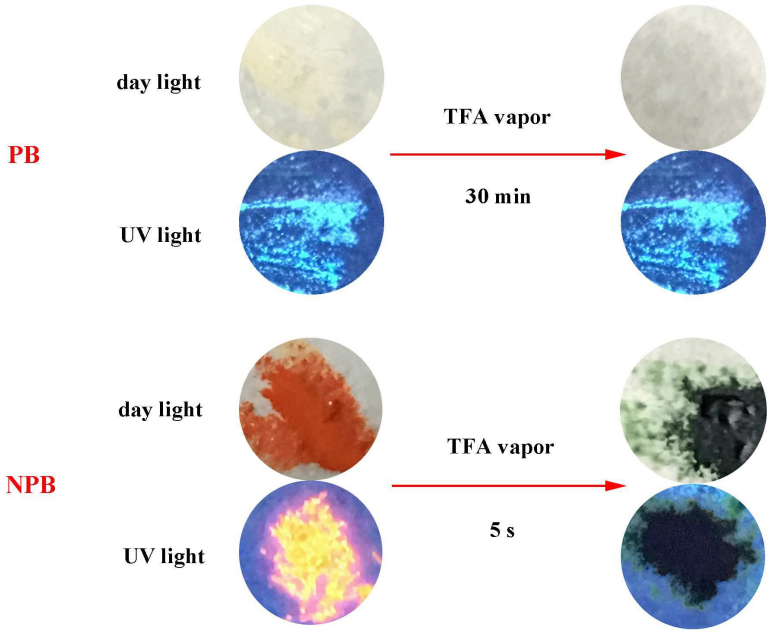

Fig. 15 Images of **PB** and **NPB** fabricated on a piece of filter paper (size: 1 cm × 1 cm) before and after fumed with TFA vapor under day light (upper) and the illumination with 365 nm UV light (lower).

View Article Online
DOI: 10.1039/C7TC03472E

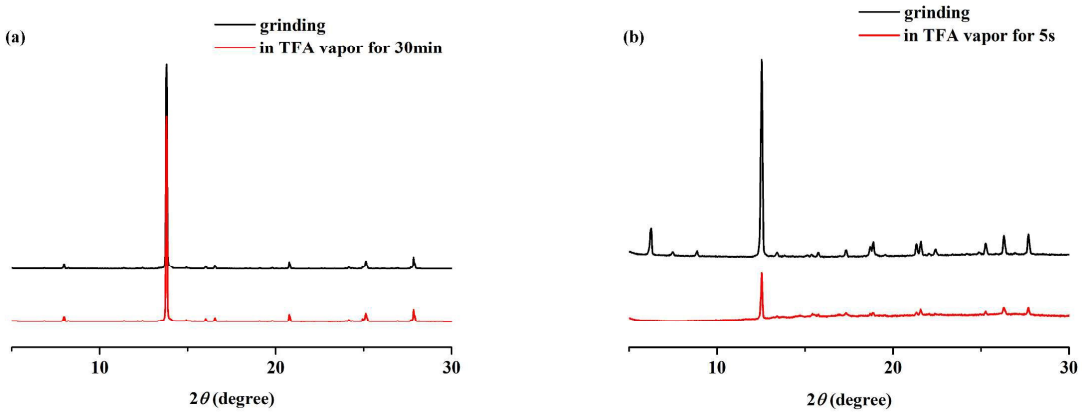

Fig. 16 PXRD patterns of (a) **PB** and (b) **NPB**.

Logic gate application

Inspired by the pH-responsive fluorescence, we employed the **PB** solution, whose positions of the emission peaks have the one-to-one corresponding relations when the amine or acid were added respectively, as a representative to construct a logic system. For most reported molecular logic gates, with the drawback of the only single signal as an output, they are just able to perform the single logic operation. In this work, on the basis of pH-mediated multisignal response, multiple logic systems can be designed by rationally defining logic states. In these logic operations, the **PB** aqueous solution served as a gate, while amine and acid were used as inputs and fluorescent signals as outputs. The presence and absence of inputs were defined as 1 and 0, respectively. Since the optical response to pH is highly reversible, construction of more useful and multiple-configurable logic gates is possible. When amine and acid were used as chemical inputs, the INH logic gate (447 nm as output) and IMPLICATION (IMP) logic gate (437 nm as output) were constructed (Fig. 17) and could display quick and sensitive optical behavior. A logic gate with two output signals may improve its stability greatly, and so far, dual-output logic gates have been barely reported,[55] thus, the logic system based on the pH-responsive **PB** with high sensitivity and fast response

View Article Online
DOI: 10.1039/C7TC03472E

could also hold potential applications in the field of material science and biomedicine.

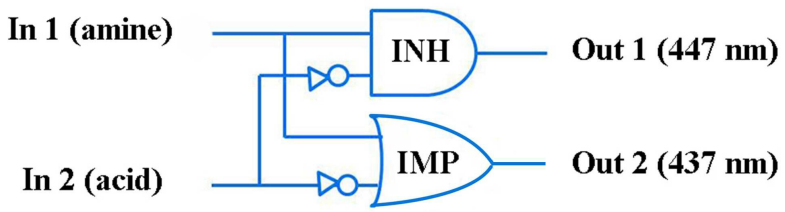

In 1 (amine)	In 2 (acid)	Out 1(447 nm)	Out 2 (437 nm)
0	0	0	1
1	0	0	1
0	1	1	0
1	1	0	1

Fig. 17 Colorimetric INH and IMP logic gates and their truth table of **PB**.

Conclusions

Two new atypical AIE chromophores **PB** and **NPB** were designed and synthesized, also characterized by IR, ^{1}H NMR, ^{13}C NMR and HRMS. Both **PB** and **NPB** showed the positive solvatochromism because of their different molecular conformations in various solvents. **PB** with two methyl groups and **NPB** with C=C bond and *N*,*N*-dimethylaniline substituting groups showed a variable red-shifted emission in their solid state due to their distinctive levels of intramolecular push-pull electronic effect. Thanks to the twisted structures, **PB** and **NPB** experienced little π-π stacking interaction in their condensed phase and therefore exhibited obvious fluorescence emission in the solid state. The density functional theory calculations indicated that the HOMO and LUMO energy levels of **PB** and **NPB** were well separated, verifying the status for both **PB** and **NPB** as D-π-A compounds. Besides, the bandgap value of **NPB** was a little lower comparing with that of **PB**, indicating its larger

View Article Online
DOI: 10.1039/C7TC03472E

delocalization and push-pull effect. Moreover, as one would expect, **PB** and **NPB** underwent a dramatic color change upon addition of acid as a result of the protonation of the nitrogen atoms. Furthermore, based on the pH-sensitive properties, a dual-output INH logic gate was developed successfully. The novel pyrimidine-phthalimide derivatives with sensitive response to pH both in water solution and in the gas phase may hold great potential for applications in the material science fields.

Experimental Section

Materials and Measurements. THF was distilled under normal pressure from sodium benzophenone ketyl under nitrogen prior to use. All chemicals were purchased from Acros or Aldrich and used as received. ^{1}H and ^{13}C NMR spectra were collected on a Bruker Spectrospin Avance 400 MHz NMR spectrometer in $CDCl_3$ with tetramethylsilane (TMS; δ = 0 ppm) as internal standard. HRMS was acquired on Micromass-GTC spectrometer. UV absorption spectra were obtained on a Varian CARY 100 Bio spectrophotometer. PL spectra were recorded on a spectrofluorophotometer (RF-5301PC, SHIMADZU, Japan). The relative fluorescence quantum yields were estimated relative to solutions of 5×10^{-5} M quinine sulfate with Φ_R = 0.55 in 0.1 M sulfuric acid solution as a standard sample. The single-crystal X-ray diffraction data for the crystals of **PB** and **NPB** prepared with 50 mg samples and 50 mL THF/water (1:1 by volume) as solvent was collected from a BRUKER D8 VENTURE system with Cu-K a radiation (l ¼ 1.54178 Å) at 280 (10) K. The structure was solved using direct methods following the difference Fourier syntheses. All non-hydrogen atoms were anisotropically refined through least-squares on F^2 using the SHELXTL program suite. The anisotropic thermal parameters were assigned to all non-hydrogen atoms. The hydrogen atoms attached to carbon were placed in idealized positions and refined using a riding model to the atom from which they were attached. The

View Article Online
DOI: 10.1039/C7TC03472E

pictures of structure were produced using Diamond 3.1. CCDC 1566171 and 1566173 contained the supplementary crystallographic data of this work. Scanning electron microscope (SEM) images were taken on a S4800 (Hitachi, Japan) scanning electron microscope. Thermogravimetric analysis (TGA) was carried out under a N_2 atmosphere at a heating rate of 10 °C/min. The ground-state geometries were optimized with the B3LYP/6-31G(d) program, using the Gaussian 03 package.

Synthetic procedures

PB. Isobenzofuran-1,3-dione (1.2 equiv) and 4,6-dimethylpyrimidin-2-amine (1.0 equiv) were added in 3 mL of dry toluene and 1-2 mL of triethylamine (TEA). The mixture was heated at 200°C for 2 h, and allowed to cool to room temperature. Further heating was conducted to remove the solvent, and the residues were purified by silica gel column chromatography, gaining a pale white solid powder **PB** (yield: 86%), mp 210.9-211.6 °C. FT-IR (ν/cm $^{-1}$): 3321, 3057, 3026, 2923, 2866, 1579, 1485, 1282, 501. ^{1}H NMR (400 MHz, $CDCl_3$) δ 7.96 (dd, J = 5.5, 3.0 Hz, 1H), 7.82-7.76 (m, 1H), 7.12 (s, 1H), 2.59 (s, 1H). ^{13}C NMR (400 MHz, $CDCl_3$) δ 134.58 (s), 124.02 (s), 119.92 (s), 23.94 (s). MS: Calculated = 254.0930, found = 254.0932 $(M+H)^+$.

NP. Compounds **NP** were synthesized according to literature method.[56]

NPB. Replacing 4,6-dimethylpyrimidin-2-amine by **NP**, compound **NPB** was obtained using similar procedure described for compound **PB** as a red solid (yield: 78%), mp 269.2-269.7 °C. FT-IR(ν/cm $^{-1}$): 3078, 2960, 2929, 2873, 1741, 1593, 1284, 1143. ^{1}H NMR (400 MHz, $CDCl_3$) δ 8.03-7.96 (m, 2H), 7.85-7.79 (m, 4H), 7.52 (d, J = 8.7 Hz, 4H), 7.26 (s, 1H), 6.94 (d, J = 15.8 Hz, 2H), 6.85-6.64 (m, 4H), 3.04 (s, 12H). ^{13}C NMR (400 MHz, $CDCl_3$) δ 166.44 (s), 165.64 (s), 153.34 (s), 150.86 (s), 138.21 (s), 134.36 (s), 132.18 (s), 129.34 (s), 123.90 (s), 120.72 (s), 113.63 (s), 112.24 (s), 40.37 (s). MS: Calculated =

View Article Online
DOI: 10.1039/C7TC03472E

516.2400, found = 516.2396 $(M+H)^+$.

Acknowledgements

This work was supported by the National Natural Science Foundation of China (NO 21374046), Program for Changjiang Scholars and Innovative Research Team in University, Open Project of State Key Laboratory of Supramolecular Structure and Materials (SKLSSM201718) and the Testing Foundation of Nanjing University.

Supporting Information

Available: Experimental details and characterization data and CIF.

References

1 Y. L. Tsai, C. C. Chang, C. C. Kang and T. C. Chang, *J. Lumin.*, 2007, **41**, 127.

2 B. Hugon, F. Anizon, C. Bailly, R. M. Golsteyn, A. P. S. Léonce, J. Hickman, B. Pfeifferc and M. Prudhomme, *Bioorg. Med. Chem.*, 2007, **15**, 5965.

3 T. Taskin and F. Sevin, *J. Mol. Struct.: Theochem.*, 2007, **61**, 803.

4 E. Conchon, F. Anizon, B. Aboab, R. M. Golsteyn, S. Léonce, B. Pfeiffer and M. Prud-homme, *Bioorg. Med. Chem.*, 2008, **16**, 4419-4430.

5 K. R. Yoon, S. O. Ko, S. M. Lee and H. Lee, *Dyes Pigm.*, 2007, **75**, 567.

6 K. R. Yoon, S. O. Ko and H. Lee, *Synthetic Met.*, 2007, **157**, 627.

7 I. K. Moon, C. S. Choi and N. Kim, *Polymer*, 2007, **48**, 3461.

8 Z. J. Zhao, X. J. Xu, X. P. Chen, X. M. Wang, P. Lu, G. Yu and Y. Q. Liu, *Tetrahedron*, 2008, **64**, 2658.

9 H. Chen, X. Xu, H. G. Yan, X. R. Cai, Y. Li, Q. Jiang and M. G. Xie, *Chin. Chem. Lett.*, 2007, **18**, 1496.

View Article Online
DOI: 10.1039/C7TC03472E

10 W. Li, J. Qiao, L. Duan, L. D. Wang and Y. Qiu, *Tetrahedron*, 2007, **63**, 10161.

11 K. R. J. Thomas, J. T. Lin, Y. T. Tao and C. W. Ko, *J. Am. Chem. Soc.*, 2001, **123**, 9404.

12 H. P. Zhao, X. T. Tao, F. Z. Wang, Y. Ren, X. Q. Sun, J. X. Yang, Y. X. Yan, D. C. Zou, X. Zhao and M. H. Jiang, *Chem. Phys. Lett.*, 2007, **439**, 132.

13 X. H. Li, J. Gui, H. Yang, W. J. Wu, F. Y. Li, H. Tian and C. H. Huang, *Inorg. Chim. Acta*, 2008, **361**, 2835-2840.

14 V. Van Dijken, J. J. A. M. Bastiaansen, N. M. M. Kiggen, B. M. W. Langeveld, C. Rothe, A. Monkman, I. Bach and P. Stössel, K. Brunner, *J. Am. Chem. Soc.*, 2004, **126**, 7718.

15 Y. H. Zhou, P. Peng, L. Han and W. J. Tian, *Synth. Met.*, 2007, **157**, 502.

16 Y. Ooyama, Y. Shimada, Y. Kagawa, Y. Yamada, I. Imae, K. Komaguchi and Y. Harima, *Tetrahedron Lett.*, 2007, **48**, 9167.

17 D. X. Li, J. G. Ren, J. F. Li, Z. W. Wang and G. M. Bo, *Dyes Pigm.*, 2001, **49**, 181.

18 D. X. Li, Z. W. Wang, Z. Q. Guo and W. D. Lan, *Dyes Pigm.*, 1998, **39**, 133.

19 Z. Q. Li, M. Siklos, N. Pucher, K. Cicha, A. Ajami, W. Husinsky, A. Rosspeintner, E. Vauthey, G. Gescheidt and Stampfl, *J. Polym. Sci. Pol. Chem.*, 2011, **49**, 3688-3699.

20 C. Hadad, S. Achelle and J. C. García-Martinez, *J. Org. Chem.*, 2011, **76**, 3837-3845.

21 J. Luo, Z. Xie, J. W. Y. Lam, L. Cheng, H. Chen and C. Qiu, *Chem. Commun.*, 2001, 1740-1741.

22 B. K. An, S. K. Kwon, S. D. Jung and S. Y. Park, *J. Am. Chem. Soc.*, 2002, **124**, 14410-14415.

23 Y. Hong, J. W. Y. Lam and B. Z. Tang, *Chem. Soc. Rev.*, 2011, **40**, 5361-5388.

24 Y. Hong, J. W. Y. Lam and B. Z. Tang, *Chem. Commun.*, 2009, 4332-4353.

25 R. Hu, N. L. C. Leung and B. Z. Tang, *Chem. Soc. Rev.*, 2014, **43**, 4494-4562.

26 X. Zhang, X. Zhang, L. Tao, Z. Chi, J. Xu and Y. Wei, *J. Mater. Chem. B*, 2014, **2**,

View Article Online
DOI: 10.1039/C7TC03472E

4398-4414.

27 J. Liang, B. Z. Tang and B. Liu, *Chem. Soc. Rev.*, 2015, **44**, 2798-2811.

28 D. Ding, K. Li and B. Liu, *Acc. Chem. Res.*, 2013, **46**, 2441-2453.

29 Z. Chi, X. Zhang, B. Xu, X. Zhou, C. Ma and Y. Zhang, *Chem. Soc. Rev.*, 2012, **41**, 3878-3896.

30 X. Zhang, Z. Chi, Y. Zhang, S. Liu and J. Xu, *J. Mater. Chem. C*, 2013, **1**, 3376-3390.

31 M. R. Rao, C. W. Liao and S. S. Sun, *J. Mater. Chem. C*, 2013, **1**, 6386-6394.

32 Y. Dong, J. Zhang, X. Tan, L. Wang, J. Chen and B. Li, *J. Mater. Chem. C*, 2013, **1**, 7554-7559.

33 Q. Qi, X. Fang, Y. Liu, P. Zhou, Y. Zhang and B. Yang, *RSC Adv.*, 2013, **3**, 16986-16989.

34 R. Zheng, X. Mei, Z. Lin, Y. Zhao, H. Yao and W. Lv, *J. Mater. Chem. C*, 2015, **3**, 10242-10248.

35 M. R. Rao, C. W. Liao, W. L. Su and S. S. Sun, *J. Mater. Chem. C*, 2013, **1**, 5491-5501.

36 J. W. Chung, B. K. An and S. Y. Park, *Chem. Mater.*, 2008, **20**, 6750-6755.

37 W. Z. Yuan, Y. Gong, S. Chen, X. Y. Shen, J. W. Y. Lam, P. Lu, Y. Lu, Z. Wang, R. Hu and N. Xie, *Chem. Mater.*, 2012, **24**, 1518-1528.

38 G. Chen, W. Li, T. Zhou, Q. Peng, D. Zhai, H. Li, W. Z. Yuan, Y. Zhang and B. Z. Tang, *Adv. Mater.*, 2015, **27**, 4496-4501.

39 R. Kannan, G. S. He, L. Yuan, F. Xu, P. N. Prasad, A. G. Dombroskie, B. A. Reinhardt, J. W. Baur, R. A. Vaia and L. S. Tan, *Chem. Mater.*, 2001, **13**, 1896-1904.

40 L. Wang, Z. Zheng, Z. Yu, J. Zheng, M. Fang and J. Wu, *J. Mater. Chem. C*, 2013, **1**, 6952-6959.

41 H. Cao, V. Chang, R. Hernandez and M. D. Heagy, *J. Org. Chem.*, 2005, **70**, 4929-4934.

View Article Online
DOI: 10.1039/C7TC03472E

42 H. J. Yen, H. Y. Lin and G. S. Liou, *Chem Mater.*, 2011, **23**, 1874-1882.

43 G. V. M. Sharma, J. J. Reddy, P. S. Lakshmi and P. R. Krishna, *Tetrahedron Lett.*, 2005, **46**, 6119-6121.

44 L. K. Wang, Z. Zheng, Z. P. Yu, J. Zheng, M. Fang, J. Y. Wu, Y. P. Tian and H. P. Zhou, *J. Mater. Chem. C*, 2013, **1**, 6952-6959.

45 K. Yasuhiro, S. Yusuke, F. Kazumasa and M. Masaki, *J. Phys. Chem. A*, 2014, **118**, 8717-8729.

46 B. R. Gao, H. Y. Wang, Y. W. Hao, L. M. Fu, H. H. Fang, Y. Jiang, L. Wang, Q. D. Chen, H. Xia, L. Y. Pan, Y. G. Ma and H. B. Sun, *J. Phys. Chem. B*, 2010, **114**, 1.

47 J. B. Zhang, B. Xu, J. L. Chen, L. J. Wang and W. J. Tian, *J. Phys. Chem. C*, 2013, **117**, 23117-23125.

48 Z. R. Grabowski, K. Rotkiewicz and W. Rettig, *Chem. Rev.*, 2003, **103**, 3899-4032.

49 S. Kothavale, A. G. Jadhav and N. Sekar, *Dyes Pigm.*, 2017, **137**, 329-341.

50 X. Y. Shen, Y. J. Wang, E. G. Zhao, W. Z. Yuan, Y. Liu, P. Lu, A. J. Qin, Y. G. Ma, J. Z. Sun and B. Z. Tang, *J. Phys. Chem. C*, 2013, **117**, 7334-7347.

51 K. Santosh, K. Ananda and G. Krishnamoorthy, *J. Phys. Chem. B*, 2015, **119**, 2330-2344.

52 P. Hohenberg and W. Kohn, *Physiol. Rev.*, 1964, **136**, 864.

53 A. Jacobson, A. Petric, D. Hogenkamp, A. Sinur and J. R. Barrio, *J. Am. Chem. Soc.*, 1996, **118**, 5572-5579.

54 H. Yan, X. Meng, B. Li, S. Ge and Y. Lu, *Dyes Pigm.*, 2017, **146**, 479-490.

55 W. Y. Xie, W. T. Huang, N. B. Li and H. Q. Luo, *Chem. Commun.*, 2012, **48**, 82-84.

56 B. Liu, X. L. Hu and J. Liu, *Tetrahedron Lett.*, 2007, **48**, 5958-5962.

View Article Online
DOI: 10.1039/C7TC03472E

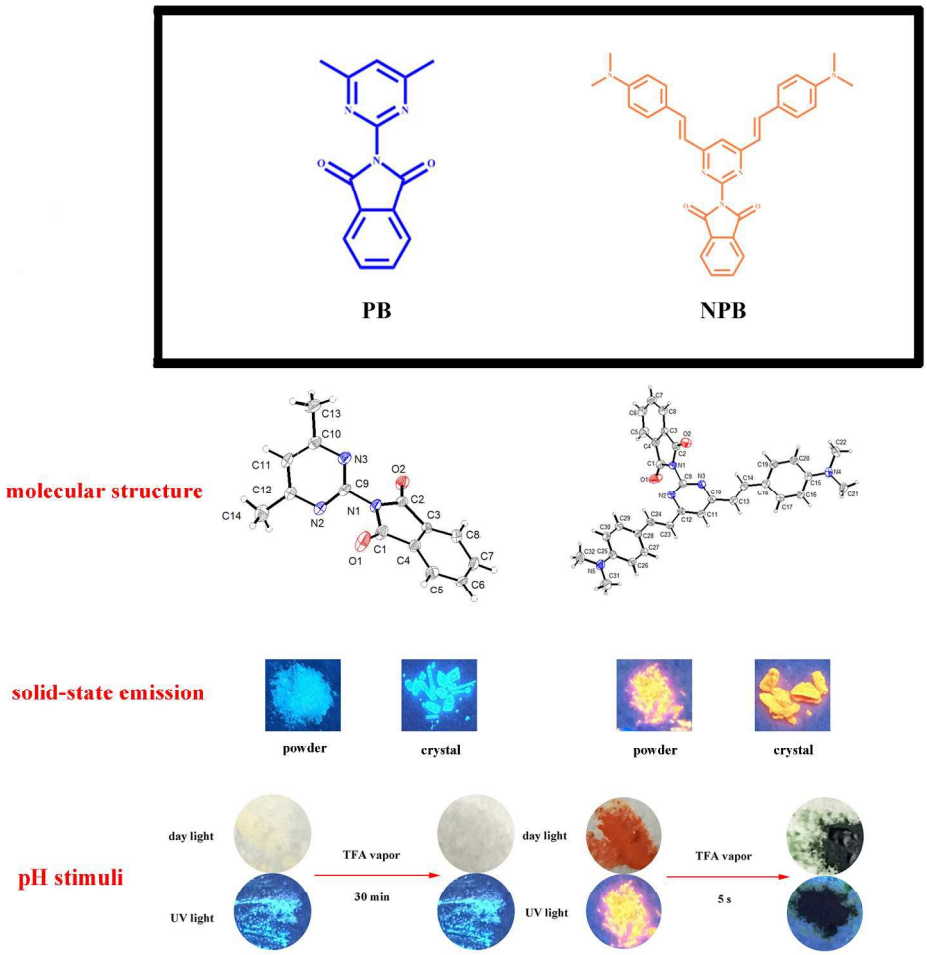

1058x1058mm (72 x 72 DPI)